2016

Closure of the macroscopic turbulence and non-equilibrium turbulent heat and mass transfer equations for porous media composed of randomly packed spheres

Furqan A. Khan
The University of Western Ontario

Anthony G. Straatman
uwo, agstraat@uwo.ca

International Journal of Heat and Mass Transfer 101 (2016) 1003–1015

Contents lists available at ScienceDirect

International Journal of Heat and Mass Transfer

journal homepage: www.elsevier.com/locate/ijhmt

Closure of a macroscopic turbulence and non-equilibrium turbulent heat and mass transfer model for a porous media comprised of randomly packed spheres

Furqan Ahmad Khan, Anthony Gerald Straatman *

Department of Mechanical & Materials Engineering, Western University, London, Ontario N6A 5B9, Canada

ARTICLE INFO

Article history:
Received 17 February 2016
Received in revised form 24 May 2016
Accepted 24 May 2016

Keywords:
Computational fluid dynamics (CFD)
Heat transfer
Mass transfer
Turbulence modeling
Porous media
Bed of spheres

ABSTRACT

Turbulent heat and mass transfer in packed beds of spheres is widely encountered in industrial and food storage applications and, as such, modeling of such cases is of interest in design and development. Herein, we propose a closure of the volume- and time-averaged (macroscopic) turbulence, and non-equilibrium turbulent heat and mass transfer equations for randomly packed spheres, based on computational results of flow and heat transfer for a unique geometric model. In this respect, the closure results are derived from pore-level (microscopic) information obtained from numerical simulations of turbulent heat and fluid flow. Turbulence is incorporated at both levels using the k–ε model, and the dispersive effects of turbulence are also considered. For the momentum equation, the closure is sought for the Darcy and Forchheimer terms. For the non-equilibrium heat and mass transport equations, we obtain closures for the dispersion, turbulent flux, turbulent dispersion, and interfacial heat and mass transfer terms. The closure results are found to be dependent upon the porosity and Reynolds number. However, the mean sphere diameter and its local variation inside the representative elemental volumes only weakly affect the results. The closure results are presented as power law-based correlations, such that they can be easily implemented in a volume-time-averaged framework.

1. Introduction

Packed beds of spheres are widely encountered in engineering applications related to the chemical processing industry, and the food storage and processing industries. The convective drying of produce stacks using warm airflow is one example of such problems. In many such applications, the sphere size is significant and heat and mass transfer are turbulent. Furthermore, it is often necessary to couple the solid and fluid phases of the process, which requires consideration of non-equilibrium heat and mass exchanges. The complex nature of such problems makes numerical modeling an attractive approach for gaining insight into the underlying physical phenomena. In this respect, turbulence modeling inside beds of packed spheres becomes critical.

Two approaches are commonly used to model the aforementioned problems. In one approach, the bed of spheres is modeled at the microscopic scale, which is characterized by the length scale of spheres. At this scale, the transport equations are used in their usual forms. However, extensive computational resources are required to model the problem. The second approach is to model the packed bed as porous continuum. By this approach, the bed of spheres is up-scaled to the macroscopic level, and the domain is considered to be comprised of solid and fluid phases with parameters like porosity and permeability describing the resistance to flow through the domain. The benefit of the macroscopic approach is that it eliminates the necessity of modeling the problem at the scale of spheres, which significantly reduces the required computational effort. However, to use this approach, the detailed information about the pore-level flow field and the energy and mass exchanges have to be determined and provided via constitutive models characterizing the porous region. The up-scaling of the mathematical formulation is carried out by volume-averaging the transport equations for mass, momentum, energy and turbulence.

The macroscopic, or volume-averaged, approach for modeling turbulent heat and mass transfer inside packed beds of spheres has been widely used for applications related to food storage and refrigeration. For example, Tapsoba et al. [1] and Moureh et al. [2,3] modeled turbulent airflow inside and around slotted-enclosures filled with spheres to understand the airflow distribution of the problem. In another study, Delele et al. [4] simulated a cold

* Corresponding author.
E-mail address: astraatman@eng.uwo.ca (A.G. Straatman).

http://dx.doi.org/10.1016/j.ijheatmasstransfer.2016.05.106
0017-9310/

Nomenclature

a_{fs}	interfacial surface area of porous media, m^2
A_{fs}	specific interfacial surface area of porous media, m^{-1}
c_E	inertial coefficient of porous media
c_p	specific heat at constant pressure in fluid region, J/(kg.K)
c_{ps}	specific heat in solid region, J/(kg.K)
$C_{1\varepsilon}$, $C_{2\varepsilon}$, C_μ	turbulence model constants
D	mass diffusivity coefficient, m^2/s
D	deformation tensor
d_s	mean sphere diameter, cm
f	body force per unit mass, m/s^2
h	specific enthalpy, J/kg
h_{fg}	latent heat of evaporation at 0 °C in fluid region, J/kg
h_{fs}	interfacial heat transfer coefficient in porous media, $W/(m^2.K)$
h_{fsm}	interfacial mass transfer coefficient in porous media, m/s
I	unit tensor
k	turbulent kinetic energy per unit mass, m^2/s^2
K	Darcy permeability of porous media, m^2
L	REV length, m
$\dot{m}$	mass flow rate, kg/s
n	unit vector normal to the surface
Nu	Nusselt number
P	pressure, Pa
Pr	Prandtl number
R	gas constant, J/(kg.K)
Re	Reynolds number
S	source in a transport equation
Sc	Schmidt number
T	temperature, °C
t	time, s
U	extrinsic velocity, m/s
v	fluid velocity vector [=(u, v, w)], m/s
Y	mass fraction
ε	dissipation rate of turbulent kinetic energy, m^2/s^3
μ_f	dynamic viscosity, $N.s/m^2$
μ_t	turbulent eddy viscosity, $N.s/m^2$
ν_f	kinematic viscosity, m^2/s
ν_t	turbulent kinematic viscosity, m^2/s
σ_T	turbulent Prandtl number for energy equation
σ_k	turbulent Prandtl number for k
σ_ε	turbulent Prandtl number for ε
ρ_s	density of solid, kg/m^3
ρ_f	density of fluid mixture, kg/m^3
λ_x	thermal conductivity of x-constituent of porous media, W/(m.K)
ϕ	porosity
φ	a quantity
$\bar{\varphi}$	time-average of φ
$\langle\varphi\rangle$	extrinsic volume-average of φ
$\langle\varphi^x\rangle$	intrinsic volume-average of φ (x is fluid or solid-constituent of porous media)
$\langle\bar{\varphi}\rangle$	volume-time-average ofφ

Subscripts and superscripts

a	air
$disp$	dispersive
eff	effective property in porous media
f	fluid
fs	interfacial
t	turbulent
v	vapor
w	water

storage room containing boxes loaded with spheres to predict airflow, temperature and humidity distribution. Similarly, the distribution of a gas used to control fruit ripening inside cold storage rooms was numerically predicted by Ambaw et al. [5]. In addition, the cooling process of packed food stacks was simulated by Alvarez and Flick [6]. All of these studies considered porous media at the macroscopic scale and modeled turbulence using eddy viscosity based models or Reynolds stress models (RSM).

To better understand the difference between the modeling approaches and the information required for the volume-averaged approach, we shift our discussion briefly to turbulence modeling using the eddy-diffusivity concept at the macroscopic scale of porous media. At the macroscopic scale, the modeling of turbulence generally involves volume- and time-averaging of the transport equations. In the volume-averaging operation, a transport equation is integrated over a Representative Elemental Volume (REV) of porous material. The volume-averaged value of a quantity φ, as described by Whitaker [7], is defined as

$$\langle\varphi\rangle = \frac{1}{V}\int_{V_f} \varphi dV \tag{1}$$

where, V refers to the volume over which the averaging process is carried out, V_f is the fluid volume inside V, and $\langle\varphi\rangle$ is defined as the extrinsic-average of φ. Using a similar approach, an intrinsic-averaged quantity $\langle\varphi\rangle^f$ is expressed as

$$\langle\varphi\rangle^f = \frac{1}{V_f}\int_{V_f} \varphi dV \tag{2}$$

The ratio $\langle\varphi\rangle/\langle\varphi\rangle^f$ then defines the porosity ϕ of porous media. Moreover, $\langle\varphi\rangle$ can be split into φ^f and its spatial deviation $\tilde{\varphi}$ as [7]

$$\varphi = \langle\varphi\rangle^f + \tilde{\varphi} \tag{3}$$

Time-averaging can also be utilized in the porous region to characterize the fluctuations of a quantity in time, similar to that done in pure fluid regions. The time-averaging of a quantity φ is give as [8]

$$\bar{\varphi} = \frac{1}{\Delta t}\int_t^{t+\Delta t} \varphi dt \tag{4}$$

Then, similar to that done for spatial deviations in Eq. (3), φ can be split into $\bar{\varphi}$ and its temporal deviation φ' as

$$\varphi = \bar{\varphi} + \varphi' \tag{5}$$

To model a quantity fluctuating in time at the macroscopic scale of porous media, both volume- and time-averaging operations are required. In this respect, Pedras and de Lemos (PDL) [8] introduced the concept of double decomposition, which involves volume-averaging followed by time-averaging or vice versa. The group showed that the order of averaging does not change the solution, i.e. $\langle\bar{\varphi}\rangle^f = \langle\bar{\varphi}\rangle^f$.

Existing literature on the macroscopic modeling of turbulence inside porous regions mainly utilizes the k–ε model, by which turbulence is characterized by the energy (k) of an average energy-containing eddy and its dissipation rate (ε). The basic derivation of the k–ε model is beyond the scope of this article, and the interested reader is directed to Wilcox [9] for a full mathematical treatment. In general, existing k–ε models can be classified based on the manner they define turbulent kinetic energy k. In this respect, early attempts made by Lee and Howell [10], Wang and Takle [11], and Antohe and Lage [12] defined the macroscopic turbulent kinetic energy k_m as [13]

$$k_m = \frac{1}{2}\overline{\langle \mathbf{v}' \rangle^f \cdot \langle \mathbf{v}' \rangle^f} \tag{6}$$

This quantity is derived by first carrying out volume-averaging of the microscopic velocity fluctuation $\mathbf{v}'$, then applying time-averaging to the square of the volume-averaged velocity fluctuation. This definition of turbulent kinetic energy was considered incomplete by Nakayama and Kuwahara (NK) [14] and PDL, both of whom defined turbulent kinetic energy k_{NK} by first squaring $\mathbf{v}'$ followed by time and volume-averaging operations. By this approach, the Reynolds-averaged Navier–Stokes (RANS) equations, along with the usual form of k and ε equations, were volume-averaged by NK and PDL to arrive at the macroscopic turbulence model. In another study, Chandesris et al. [15] used a similar approach to propose a k–ε model that characterizes turbulence inside porous media composed of pipe, channel, and rod bundles. Mathematically, k_{NK} is defined as [13]

$$k_{NK} = \frac{1}{2}\langle \overline{\mathbf{v}' \cdot \mathbf{v}'} \rangle^f \tag{7}$$

Lastly, Teruel and Rizwan-uddin (TR) [16,17] proposed a definition of turbulent kinetic energy that also includes the dispersive kinetic energy. The total macroscopic turbulent kinetic energy k_{total} is then defined as [16]

$$k_{total} = k_{NK} + \frac{1}{2}\langle \tilde{\mathbf{v}} \cdot \tilde{\mathbf{v}} \rangle^f \tag{8}$$

where the second term on the right-hand side accounts for the dispersive kinetic energy, which is considered important by TR for the porous domains having low porosity. In their work, TR applied the concept of double decomposition to the usual Navier–Stokes (N–S) equations to arrive at the velocity fluctuation in time and space, $\tilde{\mathbf{v}}'$, which was then utilized to derive k and ε equations that inherently include dispersive effects. The concept of including the dispersive portion of k and ε was taken forward by Drouin et al. [18] when the group proposed transport equations for dispersive k and ε along with k_{NK} to model turbulence.

Apart from the k–ε model, other models have also been utilized to simulate the macroscopic turbulence inside porous media. In this respect, Kuwata and Suga [19] employed the RSM to capture turbulence, especially at the fluid-porous interface. To avoid the inherent complexity of the RSM, Kuwata et al. [20] proposed a multiscale turbulence model, which utilized the transport equations of k and ε at the microscopic and macroscopic scales of porous media. Conversely, Soulaine and Quintard [21] employed a model similar to the Darcy–Forchheimer model to simulate turbulent flow in structured packings. Furthermore, a Large Eddy Simulation (LES) study was carried out by Kuwahara et al. [22] to quantify the accuracy of the k–ε model. The group found that the k–ε model can be effectively used to predict turbulent flow field inside porous media.

Based on the above discussion, it appears feasible to characterize the macroscopic turbulence inside porous media using the k–ε model. However, there is no universal form of the macroscopic k–ε model due to the presence of the additional terms that arise in the volume-averaging operation. Similarly, additional terms also arise in the volume-averaged momentum, heat and mass transport equations. Simply stated, the terms that arise in all volume-averaged equations account for the interactions between the fluid and the specific porous structure under consideration. For accurate simulation at the macroscopic level, these additional terms require closure to complete a given set of the macroscopic transport equations, and in general, this closure is achieved by simulating the problem at the microscopic scale of porous media.

At the microscopic scale, problems involving turbulent flow and heat transfer inside a bed of spheres have been extensively simulated before for various interests. Many studies [23–26] have modeled the entire bed of spheres by placing each sphere in structured manner, along with the walls containing the bed. Utilizing this approach, Guardo et al. [23] employed the various eddy viscosity based turbulence models to assess their influence on solid-to-fluid heat transfer. In continuation of their work, Coussirat et al. [24] utilized the RSM and found that it produced similar results compared to the eddy viscosity based turbulence models. Similarly, Logtenberg and Dixon [25], and Nijemeisland and Dixon [26] used the k–ε model to comprehensively examine flow and temperature fields inside a bed of spheres. To reduce the computational domain size, Jang and Chiu [27] took the advantage of symmetry to simulate the cooling process of a sintered bed of spheres.

In reality, beds of spheres are usually randomly packed, although in the existing literature very few studies consider random packing. To this end, turbulent flow inside a bed of randomly packed spheres was simulated by Ambaw et al. [5]. Similarly, Delele et al. [28] conducted the study of turbulent airflow through vented boxes containing randomly packed spheres. The group used the Discrete Element Method (DEM) to model the random arrangement of spheres. However, the aim of these studies was not to close the macroscopic model, but, to examine the flow at the pore-level.

At the microscopic scale, porous media are often modeled using a REV to reduce the computational domain. However, few studies have utilized the concept of the REV to model packed spheres at the microscopic scale. Yang et al. [29] used a REV to simulate packed beds composed of different sphere arrangements to observe their effect on turbulent flow and heat transfer. In their work, several REVs were stacked in line to produce spatially periodic flow and heat transfer in the last few downstream REVs. In another study, Gunjal et al. [30] used REVs composed of different sphere arrangements and applied periodic boundary conditions to examine the problem hydrodynamics and heat transfer. Similarly, Mathey [31] modeled turbulence and heat transfer inside a periodic domain (REV) composed of structurally packed spheres. Mathey [31] also modeled packed beds of short cylinders arranged in a random manner to achieve the more realistic packing. However, the random packing was enclosed in the tubular cylinder to mimic the case of tubular reactor.

In terms of macroscopic transport models for packed bed of spheres, we should state that none of the aforementioned microscopic scale simulation studies were focused on the closure of macroscopic models. At present, the literature shows few attempts to close such macroscopic models, even for simple two- and three-dimensional REVs. With respect to the macroscopic k–ε model, NK, PDL, and TR used two-dimensional REVs composed of structured arrays of circular and square rods. Chandesris et al. [15] and Drouin et al. [18] considered three-dimensional circular rods and flat plate arrays as their REVs. For the case of a packed bed of spheres, Alvarez and Flick [6] closed the macroscopic turbulence model using their own experimental data. Recently, Mathey [31] closed the macroscopic k–ε model for the case of structurally packed spheres. In his work, Mathey [31] also included the dispersive effects of k and ε using the model provided by TR. However, their results show the closure for only a small range of Reynolds numbers and with constant sphere packing porosity. The closure of the macroscopic energy and mass transport equations for a two-dimensional array of circular, elliptical, and square rods was carried out by De Lemos [32].

To the authors' knowledge, no existing study has proposed a closure of the macroscopic k–ε model for the case of a randomly packed bed of spheres. Moreover, no study in the existing literature has proposed a closure for the macroscopic non-equilibrium turbulent heat and mass transfer model intended for the bed of spheres. In the present work, we propose a complete closure of the macroscopic turbulence and non-equilibrium turbulent heat and mass transfer model for beds of randomly packed spheres for applications in the food storage and refrigeration industries.

Macroscopic turbulence is modeled using the k–ε model, and dispersive effects of k and ε are also considered. The macroscopic model is closed by utilizing the microscopic scale information available inside REVs of randomly packed spheres, where the REVs are produced by a recently published three-dimensional approach. The closure of the macroscopic model is extended by including parametric variations of porosity, Reynolds number and sphere diameters of practical interest. The paper is organized such that the complete macroscopic volume- and time-averaged model is presented first, followed by a discussion on the closure approach and then the microscopic results and the closure operation itself.

2. The macroscopic model

As discussed earlier, the present work is focused on the closure of a macroscopic k–ε turbulence model. To make the required turbulence closure generic, we focus on the k–ε models proposed by NK, PDL, and TR, all of which have a similar form. In general, all these models propose additional source terms in the transport equations to characterize porous region effects in the model. The only difference lies in the closure of these additional source terms. Therefore, we present a generic macroscopic k–ε turbulence model valid in the porous region.

Based on the work of NK, PDL, and TR, the volume-time-averaged mass and momentum conservation equations take the form

$$\phi\frac{\partial\langle\overline{\rho_f}\rangle^f}{\partial t}+\nabla.\left(\langle\overline{\rho_f}\rangle^f\langle\overline{\mathbf{v}}\rangle\right)=0 \tag{9}$$

$$\begin{aligned}&\frac{\partial\left(\langle\overline{\rho_f}\rangle^f\langle\overline{\mathbf{v}}\rangle\right)}{\partial t}+\frac{1}{\phi}\nabla.\left(\langle\overline{\rho_f}\rangle^f\langle\overline{\mathbf{v}}\rangle\langle\overline{\mathbf{v}}\rangle\right)\\&=-\phi\nabla\left(\langle\overline{P}\rangle^f+\frac{2}{3}\langle\overline{\rho_f}\rangle^f\langle k\rangle^f\right)+\nabla.\left[\left(\mu_f+\mu_t\right)2\langle\overline{\mathbf{D}}\rangle\right]\\&\quad+\phi\langle\overline{\rho_f}\rangle^f\overline{bff}-\frac{\phi\mu_f}{K}\langle\overline{\mathbf{v}}\rangle-\frac{\phi\langle\overline{\rho_f}\rangle^f c_E}{\sqrt{K}}|\langle\overline{\mathbf{v}}\rangle|\langle\overline{\mathbf{v}}\rangle\end{aligned} \tag{10}$$

and, $\mathbf{D}$ represents the deformation tensor defined as

$$\langle\overline{\mathbf{D}}\rangle=\frac{\mathbf{1}}{\mathbf{2}}\left[\nabla\langle\overline{\mathbf{v}}\rangle+(\nabla\langle\overline{\mathbf{v}}\rangle)^{\mathbf{T}}\right] \tag{11}$$

where, an overbar indicates a time-averaged quantity, and $\langle\ \rangle$ indicates a volume-averaged quantity. It is interesting to note that the application of volume- and time-averaging in a successive manner produces additional terms from both operations. The momentum equation, Eq. (10), uses the Boussinesq approximation to model the Reynolds stresses that arise from time-averaging, resulting in the addition of a turbulent eddy viscosity, μ_t. The last two terms on the right-hand side of Eq. (10) are closure models for terms arising from the volume-averaging operation. These two terms, which are commonly referred to as Darcy and Forchheimer terms, respectively, account for the viscous and form drag on the mean flow through the porous media.

The macroscopic k–ε equations are expressed as [8,14,16,17]

$$\begin{aligned}&\phi\frac{\partial\left(\langle\overline{\rho_f}\rangle^f\langle k\rangle^f\right)}{\partial t}+\nabla.\left(\langle\overline{\rho_f}\rangle^f\langle k\rangle^f\langle\overline{\mathbf{v}}\rangle\right)\\&=\phi\nabla.\left[\left(\mu_f+\frac{\mu_t}{\sigma_k}\right)\nabla\langle k\rangle^f\right]+P_k-\phi\langle\overline{\rho_f}\rangle^f\langle\varepsilon\rangle^f+S_k\end{aligned} \tag{12}$$

$$\begin{aligned}&\phi\frac{\partial\left(\langle\overline{\rho_f}\rangle^f\langle\varepsilon\rangle^f\right)}{\partial t}+\nabla.\left(\langle\overline{\rho_f}\rangle^f\varepsilon^f\langle\overline{\mathbf{v}}\rangle\right)=\phi\nabla.\left[\left(\mu_f+\frac{\mu_t}{\sigma_\varepsilon}\right)\nabla\langle\varepsilon\rangle^f\right]\\&\quad+C_{1\varepsilon}P_k\frac{\langle\varepsilon\rangle^f}{\langle k\rangle^f}-\phi C_{2\varepsilon}\langle\overline{\rho_f}\rangle^f\langle\varepsilon\rangle^f\frac{\langle\varepsilon\rangle^f}{k^f}+S_\varepsilon\end{aligned} \tag{13}$$

where,

$$\mu_t=C_\mu\langle\overline{\rho_f}\rangle^f\langle k\rangle^f\frac{\langle k\rangle^f}{\langle\varepsilon\rangle^f} \tag{14}$$

$$P_k=-\langle\overline{\rho_f}\rangle^f\langle\overline{\mathbf{v}'\mathbf{v}'}\rangle:\nabla\langle\overline{bf\,v}\rangle=\left(\mu_t 2\langle\overline{\mathbf{D}}\rangle-\frac{2}{3}\langle\overline{\rho_f}\rangle^f\langle k\rangle^f\mathbf{I}\right):\nabla\langle\overline{\mathbf{v}}\rangle \tag{15}$$

The terms S_k and S_ε in Eqs. (12) and (13) represent additional sources of k and ε, respectively, due to the presence of the porous media. In addition, the k–ε model constants $\sigma_k,\sigma_\varepsilon,C_\mu,C_{1\varepsilon}$, and$C_{2\varepsilon}$ have the usual values of 1.0, 1.3, 0.09, 1.44, and 1.92, respectively [9].

At this point, we shift our focus to the modeling of non-equilibrium turbulent heat and mass transfer inside the porous region. We can consider moist air as a mixture of water vapor and dry air (made of all the gaseous components). The turbulent moist air flow is solved using the aforementioned mass, momentum, and k and ε transport equations. In addition, the moisture content of the moist air is quantified by solving an additional transport equation of water vapor mass fraction Y_v . To account for the moisture gain/loss of air in the numerical model, the relevant transport equations constantly update the moist air density ρ_f by the following expression

$$\rho_f=\rho_a+\rho_v=\frac{P_a}{R_aT}+\frac{P_v}{R_vT} \tag{16}$$

where, P_a is the dry-air partial pressure, P_v is the vapor partial pressure, and R_a and $R_v$are the air and vapor gas constants, respectively. The moist air temperature T is obtained by solving its energy transport equation (see Khan et al. [33] for further details).

Since, the present work is intended for turbulent heat and mass transfer in packed bed of spheres for food storage and refrigeration applications, the present model incorporates non-equilibrium heat and mass transfer inside porous region. The heat and mass transfer of turbulent moist air flow, which forms the fluid-constituent of the porous region, is modeled using its energy transport equation and the vapor mass fraction Y_v equation. The solid-constituent, which is comprised of packed spheres, exchanges heat and mass with the moist air flow by solving separate energy and moisture transport equations. Since we consider that moisture resides in the form of water inside the spheres (food or produce), the moisture transport equation is solved for water mass fraction Y_w.

The volume-time-averaged non-equilibrium moisture equations can be expressed as

$$\begin{aligned}&\phi\frac{\partial\left(\langle\overline{\rho_f}\rangle^f\langle\overline{Y_{vf}}\rangle^f\right)}{\partial t}+\nabla.\left(\langle\overline{\rho_f}\rangle^f\langle\overline{Y_{vf}}\rangle^f\langle\overline{\mathbf{v}}\rangle\right)\\&=\nabla.\left(\langle\overline{\rho_f}\rangle^f D_{eff,f}\nabla\langle\overline{Y_{vf}}\rangle^f\right)+\phi S_{vf}+\langle\dot{m}_{fs}\rangle\end{aligned} \tag{17}$$

$$(1-\phi)\frac{\partial\left(\langle\overline{\rho_s}\rangle^s\langle\overline{Y_{w,s}}\rangle^s\right)}{\partial t}=\nabla.\left(\langle\overline{\rho_s}\rangle^s D_{eff,s}\nabla\langle\overline{Y_{w,s}}\rangle^s\right)+(1-\phi)S_{w,s}-\langle\dot{m}_{fs}\rangle \tag{18}$$

The interfacial mass transfer between the fluid and solid-constituents is modeled by $\langle\dot{m}_{fs}\rangle$ term appearing in Eqs. (17) and (18). The $\langle\dot{m}_{fs}\rangle$ term is quantified based on the quantity of water available inside the solid-constituent. The maximum value of $\langle\dot{m}_{fs}\rangle$ is evaluated as [34]

$$\langle\dot{m}_{fs}\rangle=\langle\overline{\rho_f}\rangle^f h_{fsm}A_{fs}\left(\langle\overline{Y_v}\rangle^{fs}-\langle\overline{Y_{vf}}\rangle^f\right) \tag{19}$$

where, $\langle Y_v^{fs}\rangle$ refers to the vapor mass fraction at the solid-constituent surface, which is calculated by considering the surface to be saturated with vapor; i.e. having 100% relative humidity. For

the case where the available water content is less than the $\langle \dot{m}_{fs} \rangle$ computed using Eq. (19), $\langle \dot{m}_{fs} \rangle$ is calculated based on the available water content (see Khan et al. [33] for details).

The present work also considers both the sensible and latent energy components of moist air. In this respect, the specific enthalpy of each species is given as

$$h_i = c_{p,i}T + h_{fg,i} \tag{20}$$

where, i is the species number. For the present work $i = 1$ (dry air) and 2 (water vapor), and the component of latent energy for dry air is $h_{fg,1} = 0$. Moreover, the summation of specific enthalpy of dry air and water vapor provides the total specific enthalpy of the air-vapor mixture. The volume- and time-averaged energy transport equations for the fluid and solid-constituents, respectively, are expressed as [33,35]

$$\begin{aligned}
&\sum_i \phi c_{p,i} \frac{\partial\left(\langle\overline{\rho_f}\rangle^f \langle\overline{Y_{i,f}}\rangle^f \langle\overline{T_f}\rangle^f\right)}{\partial t} + \sum_i \phi h_{fg,i} \frac{\partial\left(\langle\overline{\rho_f}\rangle^f \langle\overline{Y_{i,f}}\rangle^f\right)}{\partial t} \\
&\quad + \sum_i c_{p,i} \nabla.\left(\langle\overline{\rho_f}\rangle^f \langle\overline{Y_{i,f}}\rangle^f \langle\overline{T_f}\rangle^f \langle\overline{\mathbf{v}}\rangle\right) + \sum_i h_{fg,i} \nabla.\left(\langle\overline{\rho_f}\rangle^f \langle\overline{Y_{i,f}}\rangle^f \langle\overline{\mathbf{v}}\rangle\right) \\
&\quad = \lambda_{eff,f} \nabla^2 \langle\overline{T_f}\rangle^f + \sum_i \nabla.\left[\langle\overline{\rho_f}\rangle^f D_{eff,f} \nabla \langle\overline{Y_{i,f}}\rangle^f \left(c_{p,i}\langle\overline{T_f}\rangle^f + h_{fg,i}\right)\right] \\
&\quad + \phi S_{e,f} + h_{fs} A_{fs}\left(\langle\overline{T_s}\rangle^s - \langle\overline{T_f}\rangle^f\right)
\end{aligned} \tag{21}$$

$$\begin{aligned}
&\sum_i (1-\phi) c_{ps,i} \frac{\partial\left(\langle\overline{\rho_s}\rangle^s \langle\overline{Y_{i,s}}\rangle^s \langle\overline{T_s}\rangle^s\right)}{\partial t} \\
&\quad = \lambda_{eff,s} \nabla^2 \langle\overline{T_s}\rangle^s + \sum_i \nabla.\left[\langle\overline{\rho_s}\rangle^s D_{eff,s} \nabla \langle\overline{Y_{i,s}}\rangle^s \left(c_{ps,i}\langle\overline{T_s}\rangle^s\right)\right] \\
&\quad + (1-\phi) S_{e,s} - h_{fs} A_{fs}\left(\langle\overline{T_s}\rangle^s - \langle\overline{T_f}\rangle^f\right)
\end{aligned} \tag{22}$$

We note that the latent energy terms are not included in Eq. (22) because the solid-constituent is considered to be composed of solid-structure and water. Similar to the non-equilibrium mass transfer equations, the last two terms on the right-hand side of Eqs. (21) and (22) account for the interfacial heat transfer between the two constituents of the porous region. The sensible energy of water before evaporation is included by modeling the source term $S_{e,f} = h_{water}\langle \dot{m}_{fs} \rangle$ [36], where, h_{water} refers to the water enthalpy at the local temperature.

3. Macroscopic model closure approach

Examination of the macroscopic model (Eqs. (9) and (10), (12), (13), (17), (18), (21), (22)) presented in the last section shows that terms arising due to volume- and time-averaging of the porous region require closure to complete the model. To this end, mathematical models have been introduced for the terms in question, but coefficients are required to characterize a particular porous material. Herein, we provide a short description of the method of closure for each of the constitutive relations appearing in the momentum, turbulence, moisture and energy equations, and the information required. All information required for closure is obtained from pore-level calculations on a REV that characterizes a randomly packed bed of spheres, which will be discussed in detail in a subsequent section.

Closure of the Darcy and Forchheimer drag terms appearing in Eq. (10) is achieved by considering the pore-level hydrodynamics of the REV. The predicted pressure drop across the REV is utilized to evaluate the permeability K and inertial coefficient c_E as [37]

$$\frac{\Delta\overline{P}}{L} = \frac{\mu_f}{K}\langle\overline{\mathbf{v}}\rangle + \frac{\langle\overline{\rho_f}\rangle^f \mathbf{c_E}}{\sqrt{\mathbf{K}}} |\langle\overline{\mathbf{v}}\rangle| \langle\overline{\mathbf{v}}\rangle \tag{23}$$

where, $\Delta\overline{P}$ is the pressure drop across the length L of the REV. For each geometric model, creeping flow ($Re_d \approx 0.1$) is considered first to calculate K; then c_E is evaluated for higher Re_d.

Hydrodynamic closure is completed by closing the macroscopic k and ε equations. To achieve this, models must be implemented for the S_k and S_ε terms given in Eqs. (12) and (13), respectively. The closures for these terms proposed by NK, PDL, and TR are given in Table 1, which shows that each study has modeled them in a slightly different manner. To better understand these models, consider a REV with one-dimensional fully-developed flow and zero-mean-shear. Under such conditions, the transport terms in Eqs. (12) and (13) disappear and the equations reduce to a balance of source and sink terms. For example, the k and ε equations proposed by NK reduce to [14]

$$0 = -\phi\langle\overline{\rho_f}\rangle^f \langle\varepsilon\rangle^f + \phi\langle\overline{\rho_f}\rangle^f \varepsilon_\infty \tag{24}$$

$$0 = -\phi C_{2\varepsilon}\langle\overline{\rho_f}\rangle^f \langle\varepsilon\rangle^f \frac{\langle\varepsilon\rangle^f}{\langle k\rangle^f} + \phi C_{2\varepsilon}\langle\overline{\rho_f}\rangle^f \varepsilon_\infty \frac{\varepsilon_\infty}{k_\infty} \tag{25}$$

which, after simplifications yields

$$\langle k\rangle^f = k_\infty \text{ and } \langle\varepsilon\rangle^f = \varepsilon_\infty \tag{26}$$

The model constants k_∞ and ε_∞ can then be obtained as the intrinsic-averaged value of k and ε inside the REV. The closure of S_k and S_ε proposed by PDL and TR can also obtained in the similar manner. In addition, if one includes the dispersive effects of k and ε, then based on Eq. (8), the total turbulent kinetic energy k_{total} and its dissipation rate ε_{total} can be written as [16,17]

$$k_{total} = \langle k\rangle^f + k_{disp} \tag{27}$$

$$\varepsilon_{total} = \langle\varepsilon\rangle^f + \varepsilon_{disp} \tag{28}$$

where, k_{disp} and ε_{disp} are evaluated, using the expressions proposed by TR, as

$$k_{disp} = \frac{1}{2}\left\langle\left(\overline{\mathbf{v}} - \langle\overline{\mathbf{v}}\rangle^{\mathbf{f}}\right)^2\right\rangle^f \tag{29}$$

$$\varepsilon_{disp} = \nu_f\left\langle\frac{\partial\overline{\mathbf{v}}}{\partial x}\frac{\partial\overline{\mathbf{v}}}{\partial x} + \frac{\partial\overline{\mathbf{v}}}{\partial y}\frac{\partial\overline{\mathbf{v}}}{\partial y} + \frac{\partial\overline{\mathbf{v}}}{\partial z}\frac{\partial\overline{\mathbf{v}}}{\partial z}\right\rangle^f \tag{30}$$

Thus, the generic closure of the macroscopic k–ε turbulence model including the dispersive effects can be obtained from the solutions of the pore-level, time-averaged turbulent flow field inside the REV.

Closure of the macroscopic, non-equilibrium heat and mass transfer equations requires determination of the interfacial heat and mass transfer coefficients (h_{fs} and h_{fsm}) along with the effective thermal conductivity λ_{eff} and mass diffusivity coefficients D_{eff} given in Eqs. (17), (18), (21), and (22). Under fully-developed conditions and constant surface temperature, h_{fs} can be evaluated as [38]

$$h_{fs} = -\frac{\dot{m}c_p}{a_{fs}} ln\left(\frac{T_s - T_{out}}{T_s - T_{in}}\right) \tag{31}$$

where, a_{fs} is the interfacial surface area of the REV, $\dot{m}$ is the mass flow rate though the REV, T_s is the constant surface temperature of the solid-constituent, and T_{in} and T_{out} are the mass-averaged bulk fluid temperatures at the inlet and outlet of the REV, respectively.

Table 1
Models of S_k and S_ε proposed by NK [14], PDL [8] and TR [16,17].

Turbulent model	S_k	S_ε
NK	$\phi\langle\overline{\rho_f}\rangle^f \varepsilon_\infty$	$\phi C_{2\varepsilon}\langle\overline{\rho_f}\rangle^f \varepsilon_\infty \frac{\varepsilon_\infty}{k_\infty}$
PDL	$\frac{\phi C_k \langle\overline{\rho_f}\rangle^f \langle k\rangle^f}{\sqrt{K}} \lvert\overline{\mathbf{v}}\rvert$	$\frac{\phi C_{2\varepsilon} C_k \langle\overline{\rho_f}\rangle^f \langle\varepsilon\rangle^f}{\sqrt{K}} \lvert\overline{\mathbf{v}}\rvert$
TR	$\langle\overline{\mathbf{v}}\rangle\left(\frac{\phi\mu_f}{\mathbf{K}}\langle\overline{\mathbf{v}}\rangle + \frac{\phi\langle\overline{\rho_f}\rangle^{\mathbf{f}}\mathbf{c_E}}{\sqrt{\mathbf{K}}} \lvert\langle\overline{\mathbf{v}}\rangle\rvert\langle\overline{\mathbf{v}}\rangle\right)$	$\frac{\phi f(\phi,K)\langle\overline{\rho_f}\rangle^f \langle\varepsilon\rangle^f}{\sqrt{K}} \lvert\langle\overline{\mathbf{v}}\rangle\rvert$

For evaluation of h_{fs}, the value of T_s and T_{in} are set as boundary conditions to determine T_{out}. However, under fully-developed conditions, h_{fs} is constant, and hence independent of T_s and T_{in}.

The effective thermal conductivity of the fluid-constituent, $\lambda_{eff,f}$, arises in Eq. (21) due to volume- and time-averaging. This quantity represents the net thermal transport and is utilized in a gradient-diffusion type closure model [35]. Volume-averaging of the energy equation produces tortuosity and thermal dispersion terms, which are modeled as [35]

$$\text{Tortuosity}: \nabla.\left[\frac{1}{\Delta V}\int_{a_{fs}} \mathbf{n}\lambda_f \overline{T_f} dA\right] = \lambda_{tor}.\nabla \overline{T_f}^f \tag{32}$$

$$\text{Thermal dispersion}: -c_p\langle\overline{\rho_f}\rangle^f\left(\phi\langle\overline{\tilde{\mathbf{v}}\tilde{T}_f}\rangle^f\right) = \lambda_{disp}.\nabla\langle\overline{T_f}\rangle^f \tag{33}$$

Following on, time-averaging of the volume-averaged energy equation results in additional terms characterizing turbulent heat flux and turbulent thermal dispersion, which are closed as [35]

$$\text{Turbulent heat flux}: -c_p\langle\overline{\rho_f}\rangle^f\left(\phi\overline{\langle\mathbf{v}'\rangle^f\langle T_f'\rangle^f}\right) = \lambda_t.\nabla\langle\overline{T_f}\rangle^f \tag{34}$$

$$\text{Turbulent thermal dispersion}: -c_p\langle\overline{\rho_f}\rangle^f\left(\phi\langle\overline{\tilde{\mathbf{v}}'\tilde{T}_f'}\rangle^f\right) = \lambda_{disp,t}.\nabla\langle\overline{T_f}\rangle^f \tag{35}$$

The resulting $\lambda_{eff,f}$ is then given as [35]

$$\lambda_{eff,f} = \phi\lambda_f + \lambda_{tor} + \lambda_{disp} + \lambda_t + \lambda_{disp,t} \tag{36}$$

In the above expression, λ_f is the usual thermal conductivity of the fluid-constituent. For the present work, the Tortuosity coefficient λ_{tor} becomes zero due to the approximation of a constant T_s, while, λ_{disp} is evaluated as [32]

$$\lambda_{disp} = -\frac{c_p\langle\overline{\rho_f}\rangle^f\phi}{\nabla\langle\overline{T_f}\rangle^f}\left(\langle\overline{\mathbf{v}}\rangle - \langle\overline{\mathbf{v}}\rangle^{\mathbf{f}}\right)\left(\langle\overline{T_f}\rangle - \langle\overline{T_f}\rangle^f\right)^f \tag{37}$$

where,

$$\nabla\langle\overline{T_f}\rangle^f \approx \frac{\Delta\langle\overline{T_f}\rangle^f}{L} = \frac{\langle\overline{T_f}\rangle^f_{out} - \langle\overline{T_f}\rangle^f_{in}}{L} \tag{38}$$

where, in the present case, $\langle\overline{T_f}\rangle^f_{in}$ and $\langle\overline{T_f}\rangle^f_{out}$ represent the area-averaged temperature values at the inlet and outlet surfaces, respectively, which are easily calculated from pore-level results of the REV.

The microscopic simulation results cannot be utilized to evaluate λ_t and $\lambda_{disp,t}$. To this end, the eddy-diffusivity concept is adopted to model these coefficients as [32]

$$\lambda_t + \lambda_{disp,t} = c_p\langle\overline{\rho_f}\rangle^f\phi\frac{\nu_t}{\sigma_T} \tag{39}$$

where, ν_t is the kinematic turbulent viscosity, and σ_T is turbulent Prandtl number for the fluid-constituent energy equation. For the present work, σ_T is fixed at 0.9 [35].

Compared to $\lambda_{eff,f}$, the modeling of $\lambda_{eff,s}$, which arises in Eq. (22), is much more straightforward, and given as [35]

$$\lambda_{eff,s} = (1-\phi)\lambda_s + \lambda_{tor} \tag{40}$$

With λ_{tor} equal to zero, for the same reason as discussed earlier, $\lambda_{eff,s}$ only requires solid-constituent thermal conductivity λ_s and ϕ for evaluation.

For closure of the non-equilibrium mass transport equations, we take the advantage of heat and mass transfer analogy. In this respect, the Chilton-Colburn heat and mass transfer analogy is used to evaluate h_{fsm}. This analogy was found to be valid for the case of a packed bed of spheres by Gupta and Thodos [39]. The analogy relates h_{fs} and h_{fsm} as [40]

$$h_{fsm} = h_{fs}\left(\frac{D_f}{\lambda_f}\right)\left(\frac{Sc}{Pr}\right)^{\frac{1}{3}} \tag{41}$$

where, λ_f and D_f refer to the moist air thermal conductivity and its moisture diffusivity, respectively, and Pr and Sc represent the moist air Prandtl and Schmidt numbers, respectively.

Similar to $\lambda_{eff,f}$, the effective mass diffusivity of the fluid-constituent $D_{eff,f}$ accounts for the usual moisture diffusion, but also includes moisture dispersion, turbulent moisture flux, and turbulent mass dispersion, which are modeled as [32]

$$D_{eff,f} = \phi D_f + D_{disp} + D_t + D_{disp,t} \tag{42}$$

For evaluation of D_{disp}, the heat and mass transfer analogy is again utilized. Comparing the λ_{disp} and D_{disp} results presented by De Lemos [32] for two-dimensional structured REVs, we can propose the following approximate relation

$$\frac{\lambda_{eff,f}}{\lambda_f} \approx \frac{D_{eff,f}}{D_f} \tag{43}$$

The eddy-diffusivity concept is again employed to model D_t and $D_{disp,t}$ as [32]

$$D_t + D_{disp,t} = \frac{\nu_t}{Sc_t} \tag{44}$$

where, Sc_t is the turbulent Schmidt number, which for the present work is approximately 0.7–0.9 [41]. Finally, $D_{eff,s}$ is evaluated as $D_{eff,s} = (1-\phi)D_s$.

4. The microscopic model

This section covers the details of the microscopic (pore-level) simulations carried out to evaluate the closure coefficients using the approach described in Section 3 for the macroscopic model presented in Section 2. As mentioned earlier, closure is sought herein for a randomly packed bed of spheres. From the computational perspective, geometric modeling of an entire bed of packed spheres is not feasible. Therefore, we utilize REVs having random arrangements of spheres that characterize a small portion of a much larger packed bed. The approach adopted to create the REVs used the formulation developed by Dyck and Straatman [42], except using a modified contact law [43] that was suitable for spherical particles as opposed to spherical voids. Their approach produces three-dimensional domains of randomly packed spheres using *YADE* [44], with spatial periodicity maintained in the *x*, *y* and *z* directions. CAD models of the REVs are created using *Solidworks*™ [45] and then discretized using the *ANSYS*® Meshing™ tool [46].

The approach to generating a particular REV is to specify the number of spheres inside the REV along with their diameter (and standard deviation in the case of non-equal sized spheres), and the target porosity of the REV. The model places the spheres (so-called "primitives") inside of a three-dimensional box and then compresses the box allowing the spheres to collide and reorient until the target porosity is achieved. Though the approach can build REVs where the spheres are rigid solids, slight deformation was allowed to avoid having point contacts, which can cause issues with mesh generation in the space between the spheres. It was found that at least 50 spheres are required to ensure that the CFD results for the REV are independent of the REV size. Fig. 1 shows a sample REV comprised of 50 spheres of equal size randomly oriented to achieve a porosity of 0.47. Fig. 1a shows the randomly oriented spheres and the box that represents the REV. The spheres that are outside the box are those that penetrate the boundaries on the opposite periodic face and are simply shown to illustrate how the REV is trimmed out of the random packing.

Fig. 1b shows the portion of the REV that requires discretization for CFD simulation; i.e. the spheres are subtracted and the fluid space between them remains.

The fluid space in the REV was discretized using the *ANSYS*® Meshing™ tool [46] and pore-level simulations of the REVs were carried out using the commercial CFD software *Fluent*™ [47]. To improve the convergence and stability of the simulation, the unstructured meshes generated using the *ANSYS*® Meshing™ tool [46] were converted to polyhedral meshes using *Fluent*™. Since the meshing volume of the REV varies with porosity and sphere diameter, the grid convergence of the domain was based on the ratio of mean sphere diameter d_s to the meshing element size. Table 2 shows that grid convergence based upon normalized pressure difference, $\Delta P/L$, and normalized $\langle k \rangle^f$ and $\langle \varepsilon \rangle^f$ is achieved to within 1% when the ratio is kept to approximately 36, which required grids on the order of 2.2×10^6 cells.

For consistency, turbulence was modeled in the pore-level (microscopic) simulations using the k–ε model. As the robustness of the macroscopic closure depends on the accuracy of the microscopic simulations, different variations of the k–ε model were tested. The *Realizable* variation compared to the standard model was found to improve the solution convergence as it is better suited to flows having rotation, separation, and recirculation [48]. Moreover, the effects of curvature were incorporated in the model by applying the *curvature correction*, which modifies the turbulence production term in the k and ε equations [48]. Near-wall effects were accounted for by employing *Enhanced wall treatment*, which resolves the viscous sublayer in the finely meshed regions and employs the law-of-the-wall in the coarsely meshed areas [48]. The use of *Enhanced wall treatment* is necessary in the microscopic model because the meshed REVs have numerous regions of fine mesh, which occur near the contact regions of the spheres. Heat transfer was incorporated by solving the energy transport equation; mass transfer between and among the phases was not included in the pore-level calculations. The advection scheme *QUICK* was utilized for all the transport equations, and pressure–velocity coupling was achieved by employing the *SIMPLEC* algorithm. The convergence of the simulations was enhanced by slightly modifying the default under-relaxation factors given in *Fluent*™ [47]. Air was defined as the working fluid with constant thermophysical properties at standard temperature and pressure. The steady-state problem was simulated until the scaled residuals of all the transport equations dropped below 10^{-3}.

Periodic boundary conditions were imposed on all pairs of faces of the REV; i.e. $x\vec{x} + L$, $y\vec{y} + L$, $z\vec{z} + L$. The mass flow rate along the flow direction was used to impose a flow Reynolds number.

Table 2
Variation of the key quantities with grid convergence.

d_s/mesh element size	Cell count (million)	Normalized $\Delta P/L$	Normalized $\langle k \rangle^f$	Normalized $\langle \varepsilon \rangle^f$
10.0	0.32	63.87	2.13	25.43
23.5	0.70	65.27	2.91	37.17
28.6	1.10	65.87	3.07	39.76
33.3	1.70	66.26	3.18	41.38
36.4	2.20	67.11	3.25	42.64
40.0	2.7	67.26	3.27	42.96

Though periodic boundary conditions are imposed on all pairs of faces, we refer to the inlet and outlet faces to be those perpendicular to the flow direction. The mass flow rate is evaluated as

$$\dot{m} = \rho_f L^2 U \tag{45}$$

where, the side length L of the REV is obtained from *YADE* [44] following geometry generation, and the extrinsic flow velocity U is calculated from the Reynolds number, which is defined as

$$Re_d = \frac{\rho_f U d_s}{\mu_f} \tag{46}$$

No-slip hydrodynamic conditions were imposed at the surfaces of the spheres. In terms of energy, a mass-weighted bulk inlet temperature T_{in} was specified, and the surface temperature of the sphere surfaces inside the REV were maintained at T_s. In the present work, T_{in} and T_s were set to 5 °C and 55 °C, respectively, for all the simulations (see *Fluent*™ *Theory Guide* [48] for the details of periodic boundary condition implementation).

The developed microscopic model was validated using the results of Yang et al. [49], which focused on forced convection heat transfer in various structured beds of packed spheres. Their experimental work provides measurements of pressure drop and Nusselt number for packed beds composed of ellipsoidal and spherical particles. Measurements were obtained during the cooling process of initially heated particles. The packed bed was composed of enough particles to ensure that fully-developed flow and heat transfer occurred inside the bed. In addition, the measurements were only taken for the central packed channel to minimize the wall effects of the channel containing the bed.

To mimic this case, simple cubic packing (SC), shown in Fig. 2, and body center cubic packing (BCC) REVs based on the information provided by Yang et al. [49] were produced in *Solidworks*™ [45]. To closely match the experimental conditions, periodic boundary conditions were imposed on the REV faces normal to

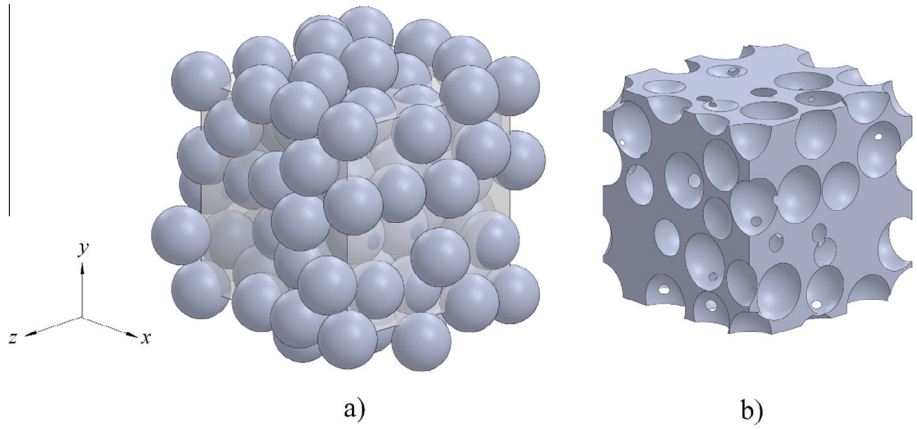

Fig. 1. (a) Geometric model showing 50 randomly oriented spheres of constant d_s and outline of REV box; (b) Resulting REV sample with porosity of 0.47.

the flow, and symmetry boundary conditions were imposed on the remaining REV faces. The flow and temperature boundary conditions were set to match the conditions provided by Yang et al. [49]. The transient problem of cooling was simplified to the steady-state based on the fact that in the fully-developed region, the Nusselt number does not change in time. The domain was discretized using the approach described earlier. The predicted pressure drop and Nusselt number for SC and BBC are shown in Figs. 3 and 4, respectively. The plots show that the present microscopic model predicts the hydraulic resistance and the heat transfer with reasonable accuracy; trends of both quantities are also correctly predicted as a function of Reynolds number. In this manner, the present model formulation is considered to be suitable and applicable to cases where the packing structure is random. In addition, comparison of Figs. 1 and 2 clearly demonstrates the inability of structured REVs (Fig. 2) to mimic the realistic random packing of spheres.

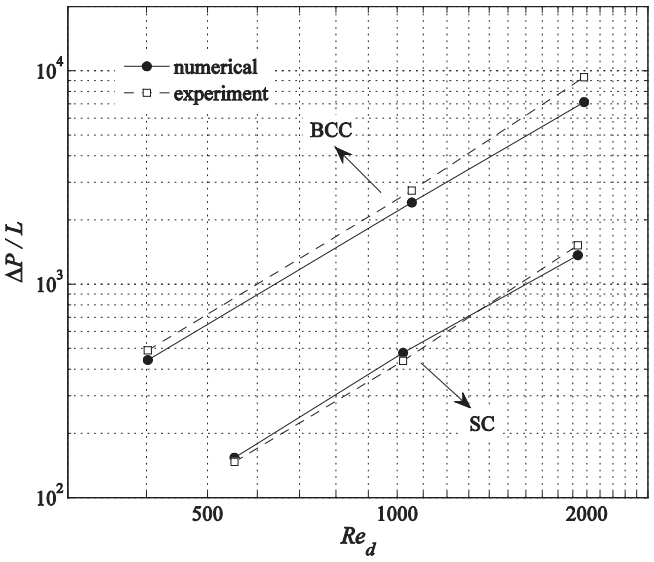

Fig. 3. Comparison of predicted pressure drop as a function of Reynolds number for different sphere packings to the experimental results of Yang et al. [49].

5. Closure results

Results of the pore-level simulations of the REVs are used in this section to close the macroscopic model presented in Section 2. Results have been obtained for 20 different geometric cases by parametrically varying the mean sphere diameter d_s (along with its statistical variation d_{var}), and porosity ϕ. The variable d_{var} defines the local variation of diameter in terms of percentage (or fraction) of d_s. For example, with $d_{var} = 20\%$, spheres inside the REV are uniformly distributed over the range $d_s \pm 0.2d_s$. As one target application of the present work is food and produce storage industry, the mean sphere diameter was varied over the range $1 \leqslant d_s \leqslant 10$ cm, which covers a wide variety of berries and nuts to apples, oranges and potatoes. Specifically, REVs considering $d_s \in \{1\text{ cm}, 5\text{ cm}, 10\text{ cm}\}$ were constructed and discretized, with local variations of sphere diameter of $d_{var} \in \{0\%, 20\%, 35\%, 50\%\}$.

The porosity of a bed of packed spheres is dependent upon the arrangement of spheres within the packing. The thinnest or loosest packing of spheres has porosity of around 0.476, while the packing of highest density produces a minimum porosity of approximately 0.26 [50]. Based on these limits, the porosity of the randomly packed REVs varied across the range $0.27 \leqslant \phi \leqslant 0.47$, specifically for the values: $\phi \in \{0.27, 0.32, 0.37, 0.42, 0.47\}$.

Table 3 gives a summary of geometric parameterization of the REVs considered herein. The side length L and the interfacial surface area a_{fs} of the generated REVs are required for various calculations, and are included in Table 3. Note that the specific interfacial surface area A_{fs} can be calculated as $A_{fs} = a_{fs}/L^3$.

As *YADE* [44] produces random packings of spheres inside the REV, each REV produced is slightly different in terms of its geometry, and within a particular REV the structure in the x, y and z directions are all slightly different, even though spatial periodicity is enforced in all principle directions. In this manner, there is no preferred direction for the prescribed flow, so each REV produced was used to simulate three cases of flow and heat transfer; one where the principle flow was prescribed in the x-direction, one for the y-direction, and one for the z-direction. The results of the three simulations were then averaged to obtain mean values for all quantities.

Finally, as fully turbulent flow is found to occur inside a porous media comprised of packed spheres when $Re_d > 300$ [8,34], to provide a wide range of applicability of the closure, the considered range of Reynolds number is $1000 \leqslant Re_d \leqslant 100{,}000$, specifically for the values: $Re_d \in \{1, 5, 10, 25, 100\} \times 10^3$. In addition, cases of

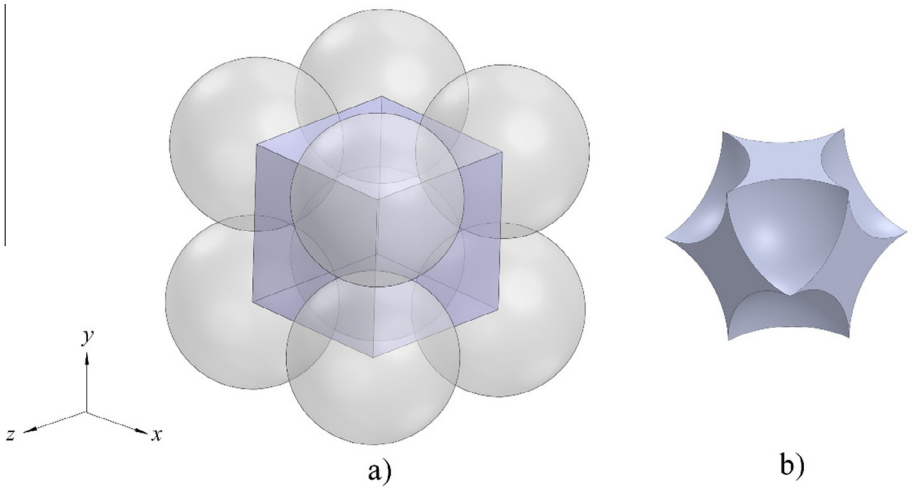

Fig. 2. (a) Box and spheres for simple cubic packing (SC); (b) Resulting SC REV sample with porosity of 0.47.

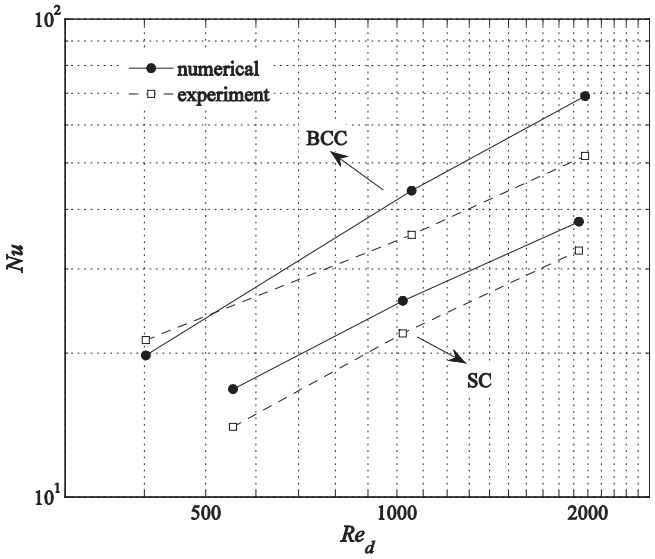

Fig. 4. Comparison of predicted Nusselt number as a function of Reynolds number for different sphere packings to the experimental results of Yang et al. [49].

Table 3
Summary of geometric parameters for the REVs produced using *YADE* [44]. Side length L and interfacial surface area a_{fs} are also given.

ϕ	d_s (cm)	d_{var} (%)	L/d_s	a_{fs}/d_s^2
0.27	10	0	3.26	114.65
0.32	10	0	3.36	129.24
0.37	10	0	3.45	139.31
0.42	10	0	3.56	147.81
0.47	10	0	3.67	150.72
0.27	5	0	3.26	114.65
0.37	5	0	3.45	139.31
0.47	5	0	3.67	150.72
0.27	1	0	3.26	114.65
0.37	1	0	3.45	139.31
0.47	1	0	3.67	150.72
0.27	10	20	3.32	123.28
0.37	10	20	3.51	141.90
0.47	10	20	3.73	156.97
0.27	10	35	3.41	125.29
0.37	10	35	3.61	147.76
0.47	10	35	3.83	160.33
0.27	10	50	3.54	131.10
0.37	10	50	3.75	156.55
0.47	10	50	3.97	168.16

$Re_d = 0.1$ were simulated to obtain the permeability of porous media. Accounting for the number of geometric models developed (Table 3), the fact that each model is run in three directions, and the range of Reynolds number considered, a total of 186 computational runs were made to produce results for the macroscopic model closure. Note that post-processing of all the simulations was also carried out using *Fluent*™ [47].

Before discussing the closure results, in Fig. 5, we present the distribution of temperature and velocity inside a typical REV to inform the reader about the complex nature of flow and other transports occurring inside the bed of packed spheres. The plot shows considerable spatial deviation in fluid temperature due to the presence of highly chaotic turbulent flow.

To obtain the closure of the volume-time-averaged momentum equation, the permeability K and inertial coefficient c_E for the Darcy and Forchheimer models are computed using the procedure described following Eq. (23). Plots of these quantities are given in Figs. 6 and 7, respectively. The permeability is found to be monotonically proportional to porosity. This trend occurs due to the increasing gaps that allow the flow to pass between the spheres more easily. On the other hand, c_E reduces with increasing porosity, due to a reduction in the intrinsic-velocity and pressure drop of the flow. It can also be observed that c_E is inversely proportional to Re_d. In addition, K and c_E are also found to be only weakly dependent upon d_{var}. The evaluated permeability was found to match well with the existing correlations for bed of packed spheres [6].

We obtain closure of the macroscopic k–ε model, given in Eqs. (12) and (13) by determining the intrinsic-averaged and dispersive components of k and ε, as shown in Eqs. (27) and (28). For clarity, the results of k and ε given in Figs. 8 and 9, respectively, only consider the parametric variation of porosity and Reynolds number. The plot of k shows that the dispersive component is considerably higher than the intrinsic-averaged component for all the cases. Mathey [31] also found such differences in magnitude between the dispersive and intrinsic-averaged components of k for the case of structurally packed spheres. Similar observations were also made by TR for two-dimensional array of square cylinders. They attribute the dispersive component of k to the presence of recirculation regions, which produce spatial deviations in velocity, and result in a high level of dispersive k as evident from Eq. (29). Conversely, the dispersive component of ε remains low compared to the intrinsic-averaged component. This observation is consistent with that of TR. It can also be observed that both components of k and ε increase with reducing porosity. This occurs due to the increasing intrinsic-averaged velocity, which ultimately increases velocity fluctuations in space and time. However, k and ε are found to be reasonably independent of Reynolds number. Moreover, these observed porosity and Reynolds number trends match with the results of NK and TR.

The total turbulent kinetic energy and dissipation rate, k_{total} and ε_{total}, are given in Figs. 10 and 11, respectively. The plots clearly show that mean sphere diameter and its local variation have an insignificant effect on the k and ε distribution. Thus, k_{total} and ε_{total} can be considered to be a function of porosity and Reynolds number.

As described in Section 3, closure of the volume-time-averaged non-equilibrium energy transport equations requires the determination of h_{fs}, λ_{disp}, and v_t. The kinematic turbulent viscosity v_t is obtained from the results of k_{total} and ε_{total} presented earlier. To make the results generic, h_{fs} is described by an interfacial Nusselt number as $Nu_{fs} = h_{fs}d_s/\lambda_f$. Figs. 12 and 13 show the results of Nu_{fs} and λ_{disp}, respectively. As expected, the value of both quantities increases significantly with the flow Reynolds number. However, Nu_{fs} and λ_{disp} show comparatively less dependence on porosity. Moreover, λ_{disp} is found to be only weakly affected by d_{var}. The evaluation of λ_{disp} also shows that thermal dispersion is considerably higher for all cases, which is similar to the higher values of k_{disp} and ε_{disp}.

The analysis of velocity, turbulence, and temperature fields inside the REVs reveal high spatial variations. As discussed earlier, the main cause of such high spatial variations is the turbulent flow inside the complex packed spheres domain, which produces complex recirculation, separation, and reattachment regions. Lastly, all the presented results are found to be independent of the mean sphere diameter d_s as shown in Figs. 6–13.

At this point, we propose a correlation for each closure variable evaluated for the macroscopic model, such that the closure results can be easily implemented in a volume-averaged porous media framework. The correlations are proposed in the form of a power law for porosity and Reynolds number because the results presented in Figs. 6–13 show logarithmic trends. Where necessary, a linear component is used to correlate d_{var}. To evaluate the

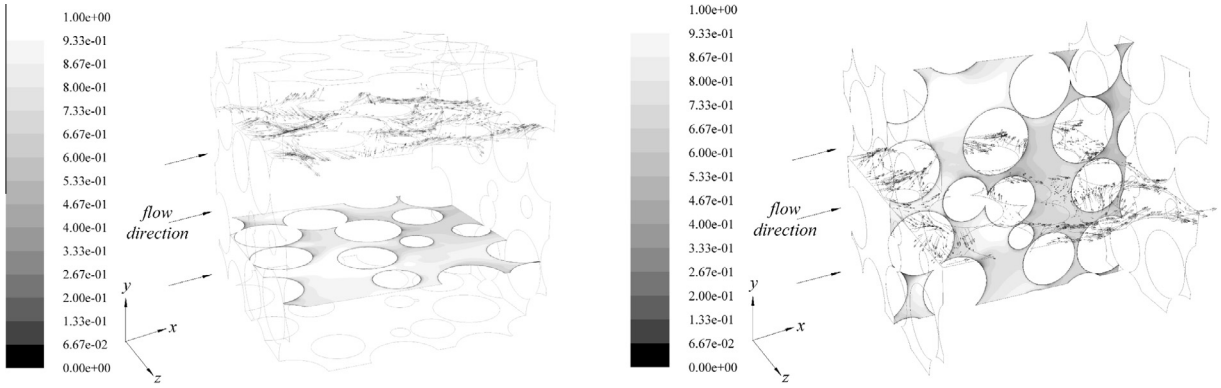

Fig. 5. Distribution of normalized fluid temperature and velocity vectors on planes inside a sample REV. Temperature is normalized as $(T - T_s)/(T_{in} - T_s)$. Results are for the case of $Re_d = 10^4$, $d_s = 10$ cm, $d_{var} = 0\%$, and $\phi = 0.47$.

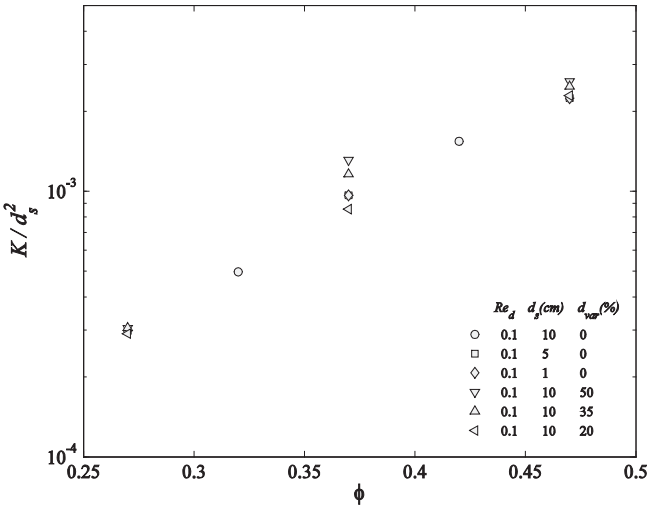

Fig. 6. Variation of permeability K with porosity, mean sphere diameter, and its local variation.

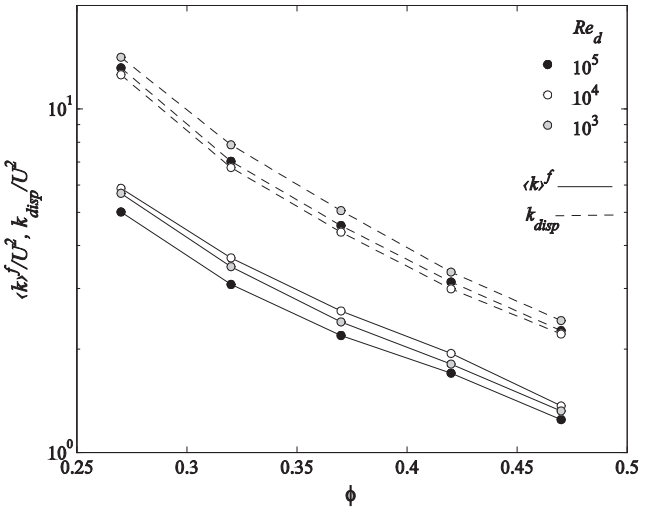

Fig. 8. Comparison of the dispersive and intrinsic-averaged components of k as a function of porosity and Reynolds number. The mean sphere diameter and its local variation inside the REVs are equal to 10 cm and 0%, respectively.

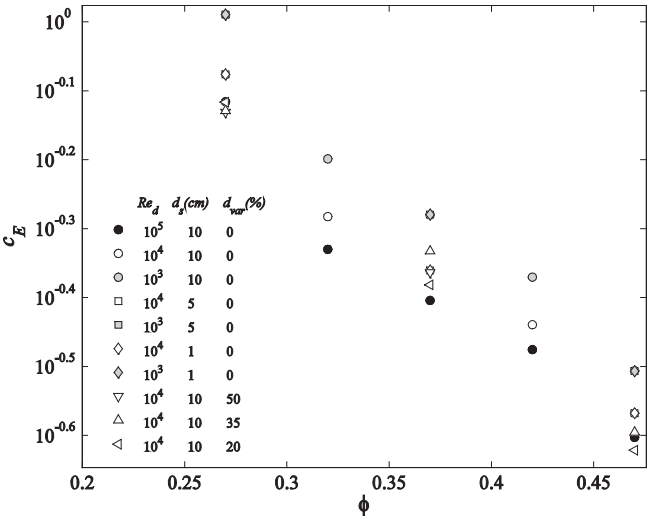

Fig. 7. Variation of inertial coefficient c_E with porosity, Reynolds number, mean sphere diameter, and its local variation.

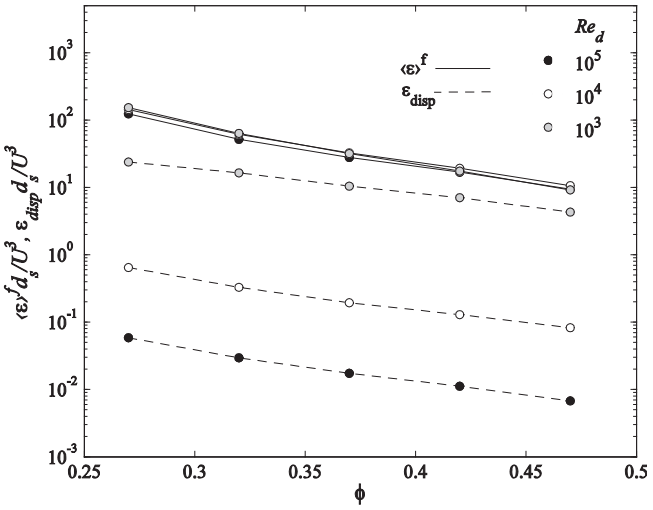

Fig. 9. Comparison of the dispersive and intrinsic-averaged components of ε as a function of porosity and Reynolds number. The mean sphere diameter and its local variation inside the REVs are equal to 10 cm and 0%, respectively.

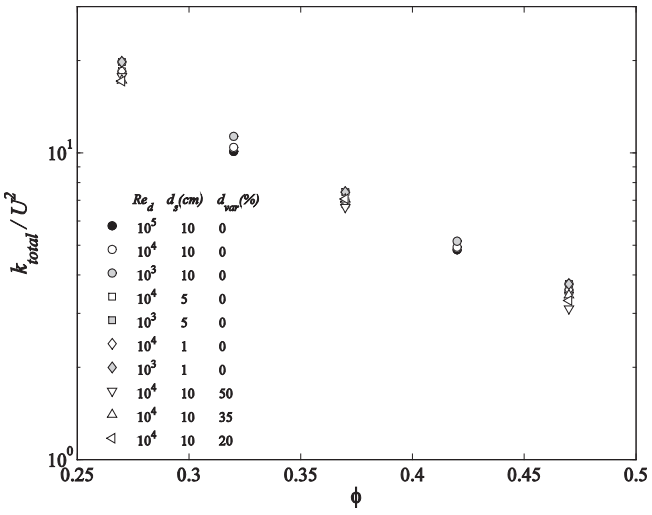

Fig. 10. Variation of the total turbulent kinetic energy k_{total} with porosity, Reynolds number, mean sphere diameter, and its local variation.

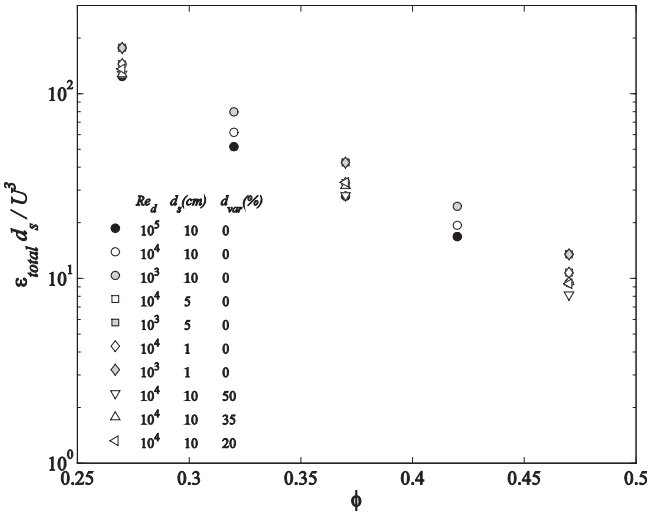

Fig. 11. Variation of the total dissipation rate of turbulent kinetic energy ε_{total} with porosity, Reynolds number, mean sphere diameter, and its local variation.

correlations, the MATLAB Curve/Surface Fitting Toolbox™ was used, which utilizes the method of least squares to fit the data. The evaluated correlations are given in Table 4. For all the closure variables, values obtained from the simulations are plotted as a function of the value predicted from the proposed correlation in Fig. 14. The plots show that power law-based correlations provide reasonable predictions for all variables. Though in some cases, second degree polynomial-based correlations more accurately predict the values, power law correlations were selected because of their conciseness.

Heat transfer inside the packed beds has been extensively studied. Since we have proposed a Nu_{fs} correlation, it is worth comparing the correlation and the obtained results against the existing Nu_{fs} literature. In this respect, the correlations and their derived results proposed by Wakao et al. [51], Gillespie et al. [52] and Achenbach [53] were found to be in the similar range as proposed by the present work.

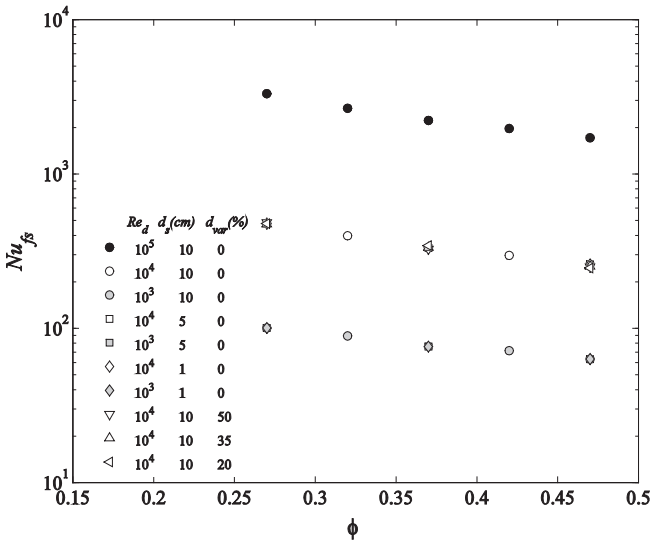

Fig. 12. Variation of interfacial Nusselt number Nu_{fs} with porosity, Reynolds number, mean sphere diameter, and its local variation.

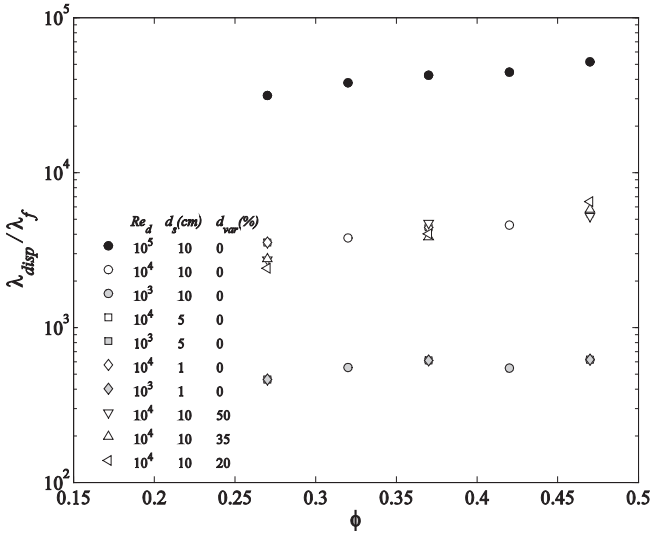

Fig. 13. Variation of thermal dispersion coefficient λ_{disp} with porosity, Reynolds number, mean sphere diameter, and its local variation.

Table 4
Proposed correlations for $k_{total}, \varepsilon_{total}, K, c_E, Nu_{fs}$, and λ_{disp}.

Closure variable	Proposed closure correlation
Total turbulent kinetic energy k_{total}	$\frac{k_{total}}{U^2} = 0.424\,\phi^{-3.084} Re_d^{-0.029}$
Total dissipation rate of turbulent kinetic energy ε_{total}	$\frac{\varepsilon_{total} d_s}{U^3} = 0.818\,\phi^{-4.59} Re_d^{-0.0916}$
Permeability of porous media K	$\frac{K}{d_s^2} = 0.0335\,\phi^{3.58} + \left(3.063 \times 10^{-6}\right) d_{var}$
Inertial coefficient of porous media c_E	$c_E = 0.103\,\phi^{-2.054} Re_d^{-0.064} - 0.001 d_{var}$
Interfacial Nusselt number Nu_{fs}	$Nu_{fs} = 0.142\,\phi^{-1.07} Re_d^{0.746}$
Thermal dispersion coefficient λ_{disp}	$\frac{\lambda_{disp}}{\lambda_f} = 1.59\,\phi^{0.8} Re_d^{0.953} + 10.0 d_{var}$

6. Summary

The present study focused on the closure of the macroscopic turbulence, and non-equilibrium turbulent heat and mass transfer model inside porous media composed of randomly packed spheres.

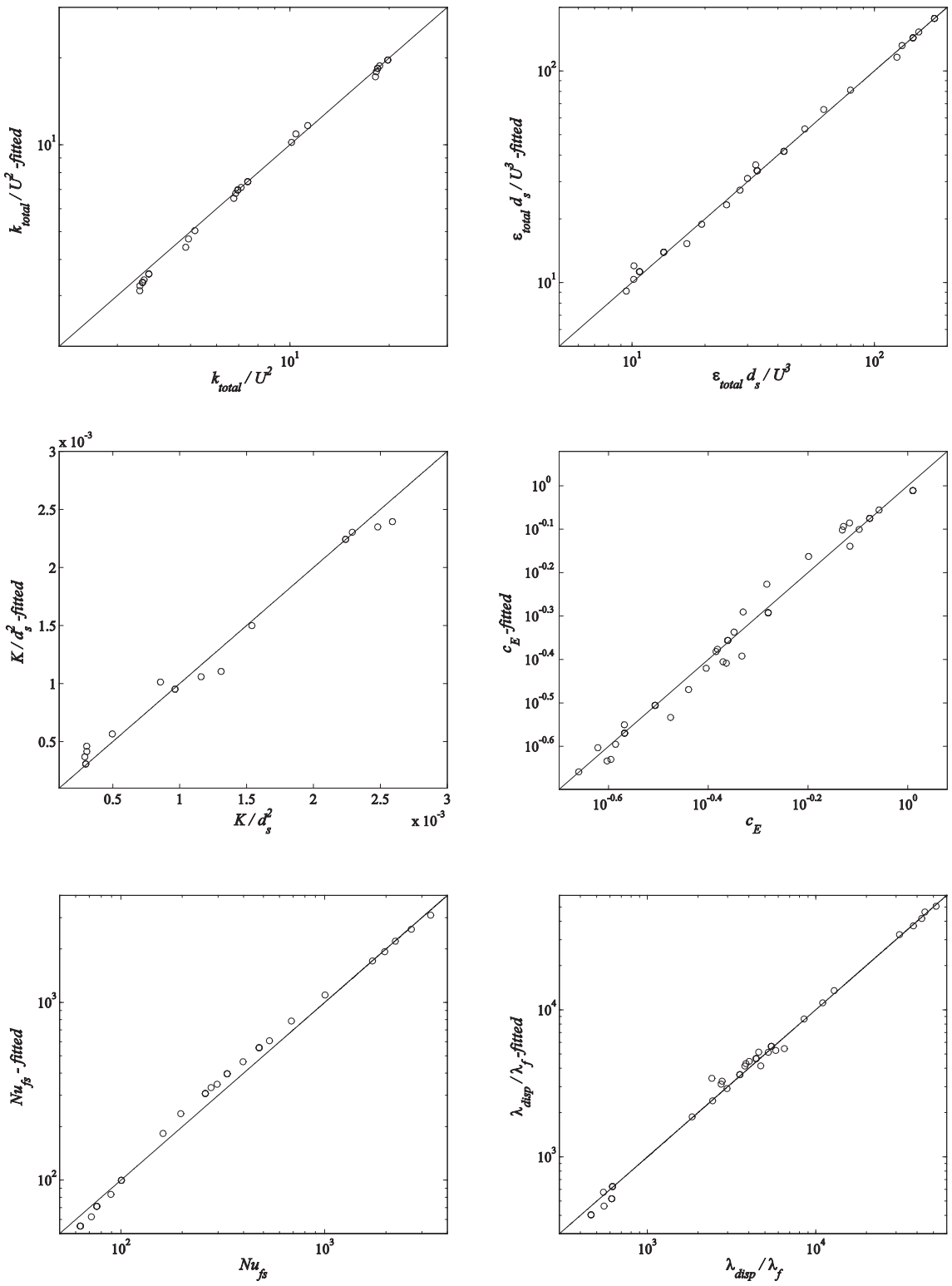

Fig. 14. Comparison of the correlations given in Table 4 versus the values of $k_{total}, \varepsilon_{total}, K, c_E, Nu_{fs}$, and λ_{disp} obtained from the numerical simulations.

The closures were required to model the additional terms that arise due to volume- and time-averaging of the transport equations. The closure of Darcy and Forchheimer terms appearing in the momentum equation required determination of porous media permeability and its inertial coefficient. For the non-equilibrium heat and mass transport equations, interfacial heat and mass transfer coefficients were needed to close the interfacial heat and mass transfer terms, respectively. Using a gradient-diffusion type model, closures were also obtained for the heat and mass transfer terms for dispersion, turbulent flux, and turbulent dispersion. The macroscopic turbulence inside porous media was modeled using the k–ε model. The dispersive effects of k and ε were also included to entirely capture the turbulence flow field.

The macroscopic model closure was obtained by simulating the problem at the pore-level or microscopic scale. In this respect, the REVs composed of randomly arranged spheres were subjected to turbulent flow and heat transfer. The conditions of fully-developed unidirectional flow with zero-mean-shear were employed to obtain the closure using the solution fields available at the microscopic scale. The developed microscopic scale model was validated using the experimental data of pressure drop and Nusselt number. The parametric variation of porosity, Reynolds number, mean sphere diameter and its local variation inside the REVs was carried out to increase the applicability of the closure results. In general, all the closure variables were found to be dependent upon the porosity and Reynolds number. However, the mean sphere diameter did not change the results. While, the local variation in spheres' diameter weakly effected the results. Lastly, the closure results were fitted using the power law-based correlations for ease of implementation into a volume-averaged framework.

Acknowledgements

The authors gratefully acknowledge the financial support from the Natural Sciences and Engineering Research Council of Canada (NSERC).

References

[1] M. Tapsoba, J. Moureh, D. Flick, Airflow patterns in an enclosure loaded with slotted pallets, Int. J. Refrig. 29 (6) (2006) 899–910.
[2] J. Moureh, M. Tapsoba, D. Flick, Airflow in a slot-ventilated enclosure partially filled with porous boxes: Part I-Measurements and simulations in the clear region, Comput. Fluids 38 (2) (2009) 194–205.
[3] J. Moureh, M. Tapsoba, D. Flick, Airflow in a slot-ventilated enclosure partially filled with porous boxes: Part II–Measurements and simulations within porous boxes, Comput. Fluids 38 (2) (2009) 206–220.
[4] M.A. Delele, A. Schenk, E. Tijskens, H. Ramon, B.M. Nicolaï, P. Verboven, Optimization of the humidification of cold stores by pressurized water atomizers based on a multiscale CFD model, J. Food Eng. 91 (2) (2009) 228–239.
[5] A. Ambaw, P. Verboven, T. Defraeye, E. Tijskens, A. Schenk, U.L. Opara, B.M. Nicolai, Porous medium modeling and parameter sensitivity analysis of 1-MCP distribution in boxes with apple fruit, J. Food Eng. 119 (1) (2013) 13–21.
[6] G. Alvarez, D. Flick, Modelling turbulent flow and heat transfer using macro-porous media approach used to predict cooling kinetics of stack of food products, J. Food Eng. 80 (2) (2007) 391–401.
[7] S. Whitaker, Volume averaging of transport equations, in: Chap. 1, Fluid Transport in Porous Media, Springer-Verlag, Southampton, UK, 1997, pp. 1–59.
[8] M.H. Pedras, M.J. de Lemos, Macroscopic turbulence modeling for incompressible flow through undeformable porous media, Int. J. Heat Mass Transfer 44 (6) (2001) 1081–1093.
[9] D.C. Wilcox, Turbulence Modeling for CFD, vol. 2, DCW industries, La Canada, CA, 1998. pp. 103–217.
[10] K. Lee, J.R. Howell, Forced convective and radiative transfer within a highly porous layer exposed to a turbulent external flow field. In: Proceedings of the 1987 ASME-JSME Thermal Engineering Joint Conf., vol. 2, 1987, pp. 377–386.
[11] H. Wang, E.S. Takle, Boundary-layer flow and turbulence near porous obstacles, Bound. Layer Meteorol. 74 (1–2) (1995) 73–88.
[12] B.V. Antohe, J.L. Lage, A general two-equation macroscopic turbulence model for incompressible flow in porous media, Int. J. Heat Mass Transfer 40 (13) (1997) 3013–3024.
[13] M.H. Pedras, M.J. de Lemos, On the definition of turbulent kinetic energy for flow in porous media, Int. Commun. Heat Mass Transfer 27 (2) (2000) 211–220.
[14] A. Nakayama, F. Kuwahara, A macroscopic turbulence model for flow in a porous medium, J. Fluids Eng. 121 (2) (1999) 427–433.
[15] M. Chandesris, G. Serre, P. Sagaut, A macroscopic turbulence model for flow in porous media suited for channel, pipe and rod bundle flows, Int. J. Heat Mass Transfer 49 (15) (2006) 2739–2750.
[16] F.E. Teruel, Rizwan-uddin, A new turbulence model for porous media flows. Part I: Constitutive equations and model closure, Int. J. Heat Mass Transfer 52 (19) (2009) 4264–4272.
[17] F.E. Teruel, Rizwan-uddin, Numerical computation of macroscopic turbulence quantities in representative elementary volumes of the porous medium, Int. J. Heat Mass Transfer 53 (23) (2010) 5190–5198.
[18] M. Drouin, O. Grégoire, O. Simonin, A consistent methodology for the derivation and calibration of a macroscopic turbulence model for flows in porous media, Int. J. Heat Mass Transfer 63 (2013) 401–413.
[19] Y. Kuwata, K. Suga, Modelling turbulence around and inside porous media based on the second moment closure, Int. J. Heat Fluid Flow 43 (2013) 35–51.
[20] Y. Kuwata, K. Suga, Y. Sakurai, Development and application of a multi-scale k–ε model for turbulent porous medium flows, Int. J. Heat Fluid Flow 49 (2014) 135–150.
[21] C. Soulaine, M. Quintard, On the use of a Darcy–Forchheimer like model for a macro-scale description of turbulence in porous media and its application to structured packings, Int. J. Heat Mass Transfer 74 (2014) 88–100.
[22] F. Kuwahara, T. Yamane, A. Nakayama, Large eddy simulation of turbulent flow in porous media, Int. Commun. Heat Mass Transfer 33 (4) (2006) 411–418.
[23] A. Guardo, M. Coussirat, M.A. Larrayoz, F. Recasens, E. Egusquiza, Influence of the turbulence model in CFD modeling of wall-to-fluid heat transfer in packed beds, Chem. Eng. Sci. 60 (6) (2005) 1733–1742.
[24] M. Coussirat, A. Guardo, B. Mateos, E. Egusquiza, Performance of stress-transport models in the prediction of particle-to-fluid heat transfer in packed beds, Chem. Eng. Sci. 62 (23) (2007) 6897–6907.
[25] S.A. Logtenberg, A.G. Dixon, Computational fluid dynamics studies of fixed bed heat transfer, Chem. Eng. Process. 37 (1) (1998) 7–21.
[26] M. Nijemeisland, A.G. Dixon, CFD study of fluid flow and wall heat transfer in a fixed bed of spheres, AIChE J. 50 (5) (2004) 906–921.
[27] J.Y. Jang, Y.W. Chiu, 3-D Transient conjugated heat transfer and fluid flow analysis for the cooling process of sintered bed, Appl. Therm. Eng. 29 (14) (2009) 2895–2903.
[28] M.A. Delele, E. Tijskens, Y.T. Atalay, Q.T. Ho, H. Ramon, B.M. Nicolaï, P. Verboven, Combined discrete element and CFD modelling of airflow through random stacking of horticultural products in vented boxes, J. Food Eng. 89 (1) (2008) 33–41.
[29] J. Yang, Q. Wang, M. Zeng, A. Nakayama, Computational study of forced convective heat transfer in structured packed beds with spherical or ellipsoidal particles, Chem. Eng. Sci. 65 (2) (2010) 726–738.
[30] P.R. Gunjal, V.V. Ranade, R.V. Chaudhari, Computational study of a single-phase flow in packed beds of spheres, AIChE J. 51 (2) (2005) 365–378.
[31] F. Mathey, Numerical up-scaling approach for the simulation of heat-transfer in randomly packed beds, Int. J. Heat Mass Transfer 61 (2013) 451–463.
[32] M.J. De Lemos, Turbulence in Porous Media: Modeling and Applications, Elsevier, 2012.
[33] F.A. Khan, C. Fischer, A.G. Straatman, Numerical model for non-equilibrium heat and mass exchange in conjugate fluid/solid/porous domains with application to evaporative cooling and drying, Int. J. Heat Mass Transfer 80 (2015) 513–528.
[34] M. Kaviany, Principles of Heat Transfer in Porous Media, Second ed., Springer-Verlag, New York, NY, 1995.
[35] M.B. Saito, M.J. de Lemos, A macroscopic two-energy equation model for turbulent flow and heat transfer in highly porous media, Int. J. Heat Mass Transfer 53 (11) (2010) 2424–2433.
[36] Y.A. Cengel, M.A. Boles, Thermodynamics an Engineering Approach, Sixth ed., McGraw Hill Company, New York, NY, 2008, pp. 738–747.
[37] S. Whitaker, The Forchheimer equation: a theoretical development, Transp. Porous Media 25 (1) (1996) 27–61.
[38] F. Incropera, D. Dewitt, T. Bergman, A. Lavine, Fundamentals of Heat and Mass Transfer, 5th ed., Wiley, Hoboken, NJ, 2006.
[39] A.S. Gupta, G. Thodos, Direct analogy between mass and heat transfer to beds of spheres, AIChE J. 9 (6) (1963) 751–754.
[40] B.R. Bird, W.E. Stewart, E.N. Lightfoot, Transport Phenomena, Second ed., John Wiley & Sons Inc, Madison, Wisconsin, 2007, pp. 582–584.
[41] Y. Tominaga, T. Stathopoulos, Turbulent Schmidt numbers for CFD analysis with various types of flowfield, Atmos. Environ. 41 (37) (2007) 8091–8099.
[42] N.J. Dyck, A.G. Straatman, A new approach to digital generation of spherical void phase porous media microstructures, Int. J. Heat Mass Transfer 81 (2015) 470–477.
[43] P.A. Cundall, O.D. Strack, A discrete numerical model for granular assemblies, Geotechnique 29 (1) (1979) 47–65.
[44] V. Smilauer, B. Chareyre, Yade dem formulation, first ed., in: V. Smilauer (Ed.), Yade Documentation, 2010.
[45] Dassault Systemes, Solidworks Educational Version 2012–2013.
[46] ANSYS, Workbench Meshing Tool, vol. 15.0.
[47] ANSYS, Fluent, vol. 14.5.
[48] ANSYS Fluent Theory Guide (2015). ANSYS Inc., Canonsburg, PA.
[49] J. Yang, J. Wang, S. Bu, M. Zeng, Q. Wang, A. Nakayama, Experimental analysis of forced convective heat transfer in novel structured packed beds of particles, Chem. Eng. Sci. 71 (2012). 126-13.
[50] F.A. Dullien, Porous Media: Fluid Transport and Pore Structure, Academic press, 2012.
[51] N. Wakao, S. Kaguei, T. Funazkri, Effect of fluid dispersion coefficients on particle-to-fluid heat transfer coefficients in packed beds: correlation of Nusselt numbers, Chem. Eng. Sci. 34 (3) (1979) 325–336.
[52] B.M. Gillespie, E.D. Crandall, J.J. Carberry, Local and average interphase heat transfer coefficients in a randomly packed bed of spheres, AIChE J. 14 (3) (1968) 483–490.
[53] E. Achenbach, Heat and flow characteristics of packed beds, Exp. Thermal Fluid Sci. 10 (1) (1995) 17–27.